Mon. Not. R. Astron. Soc. **000**, 1–6 (2000) Printed 1 February 2008 (MN LATEX style file v1.4)

Spectroscopic evidence for the binary nature of AM CVn

G. Nelemans[1], D. Steeghs[2], P. J. Groot[3]

[1] *Astronomical Institute, University of Amsterdam, Kruislaan 403, 1098 SJ, Amsterdam, The Netherlands* (gijsn@astro.uva.nl)
[2] *Astronomy Group, University of Southampton, Highfield, Southampton, SO17 1BJ, UK* (ds@astro.soton.ac.uk)
[3] *Harvard-Smithsonian Center for Astrophysics, 60 Garden St., Cambridge, MA 02138, USA* (pgroot@cfa.harvard.edu)

Received 1 February 2008

ABSTRACT

We analysed archival spectroscopic data of AM CVn taken with the William Herschel Telescope in 1996. In the literature two orbital periods for AM CVn are proposed. A clear S-wave in the He I 4471, 4387 and 4143 Å lines is revealed when the spectra are folded on the 1029 s period. No signature of this S-wave is seen when folded on 1051 s. Doppler tomography of the line profiles shows a clear signature of the hotspot. Using this we can constrain the value of K_2 to lie between 210 and 280 km s^{-1}. Our work confirms the binary nature of AM CVn beyond any doubt, establishes 1028.73 s as the true orbital period and supports the interpretation of AM CVn as a permanent superhump system.

Key words: accretion, accretion discs – novae, cataclysmic variables – binaries: close – binaries: spectroscopic – stars: individual: AM CVn

1 INTRODUCTION

AM CVn (HZ 29) was found as a faint blue object by Humason & Zwicky (1947) and shows broad He I absorption lines (Greenstein & Matthews, 1957) and no hydrogen. Periodic brightness variations on a period of ∼18 min. (Smak, 1967) and flickering (Warner & Robinson, 1972) suggested mass transfer in a very compact binary. A model in which a degenerate helium white dwarf transfers helium to another white dwarf, driven by the loss of angular momentum due to gravitational wave radiation was proposed by Paczyński (1967) and Faulkner, Flannery & Warner (1972). See for details on the models for AM CVn stars and a list of the 8 currently known systems Nelemans et al. (2001).

Since the discovery of the periodic brightness variations and the flickering, AM CVn has been extensively studied with high speed photometry (e.g Skillman et al., 1999; Solheim et al., 1998) yielding multiple periodicities on 1051, 1011 and 1029 s (see also Solheim et al., 1991; Harvey et al., 1998). Spectroscopic observations (Patterson, Halpern & Shambrook, 1993) show a 13.38 hr periodicity in the skewness of the He I absorption lines.

According to Solheim et al. (1998) the dominant 1051 s photometric period is the orbital period and the 1029 s a beat between the orbital period and the 13.38 hr precession period of the accretion disc. However, Skillman et al. (1999) argue that 1029 s is the orbital period and 1051 s is the beat period. In the latter case, the system would be similar to the permanent superhump systems among the hydrogen rich cataclysmic variables (Skillman et al., 1999).

To discern between these two possibilities and to establish beyond doubt the binary nature of AM CVn, a spectroscopic signature at either period is needed. In this article we describe a spectroscopic study of AM CVn in which we found a clear signature on the 1029 s period, proving that this is the orbital period of the system.

2 DATA REDUCTION

We analysed archival spectroscopic data obtained on the 4.2m William Herschel Telescope on February 26 and 27, 1996, with the ISIS spectrograph. In the first night a dichroic was used with both the ISIS red and blue arm. Because of ripples in the blue part of the spectrum introduced by the dichroic, it was removed on the second night and only blue spectra were taken. Because of the ripples and the lack of flat-fields of high quality for the first night we mainly discuss the data taken on the second night. In the blue arm the spectra were obtained with the R600B grating covering 3960-4760 Å at a resolution of 2.0 Å.

There are 403 spectra taken on the second night (173 on the first), each with an integration time of 30 s. Wavelength calibration lamp exposures were taken approximately every 50 spectra (about every 40 minutes). The spectra were reduced using the standard data reduction package MIDAS. After bias subtraction and flatfielding the spectra were extracted and wavelength calibrated. The wavelength calibration was very stable (less than half a pixel change between the subsequent arc spectra) and the calibration of each arc spectrum was used for the 25 spectra taken before and the 25 spectra taken after the arc without interpolation. The

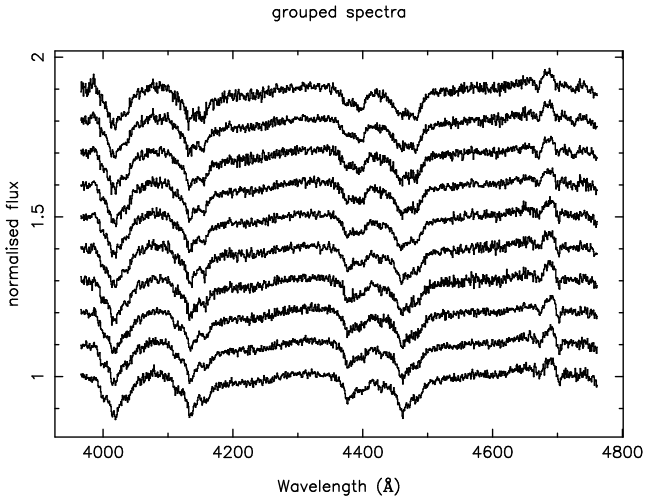

Figure 1. Spectra of the second night averaged into 10 groups of 40 consecutive spectra added together after normalising the continuum. The spectra show the change in the shape of the absorption lines over the 5 hours of the observation (see Sect. 3.4).

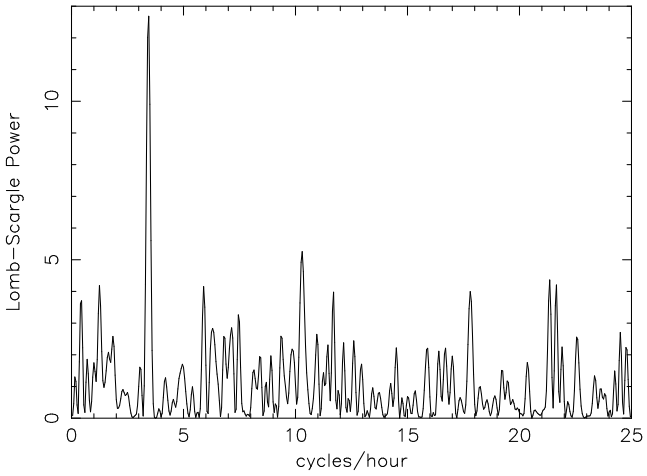

Figure 2. Lomb-Scargle power spectrum of the equivalent width lightcurve of the 4 strongest He I lines. The peak at 3.5 cycles/hour points to an orbital period around 1030s.

flat-field for the first night was taken at the beginning of the second night and had to be corrected for a small wavelength shift.

The continuum of the wavelength calibrated spectra was fitted with a cubic spline of order 3 to line-free areas and used to normalise all spectra with respect to their continuum level. In Fig. 1 we show the resulting spectra of the second night after averaging them into 10 groups over the whole night.

3 DATA ANALYSIS

3.1 A period search

In order to search for line profile variations on the uncertain orbital period of the binary, an equivalent width (EW) lightcurve was constructed using the combined EW of the four strongest He I lines. A Lomb-Scargle power spectrum

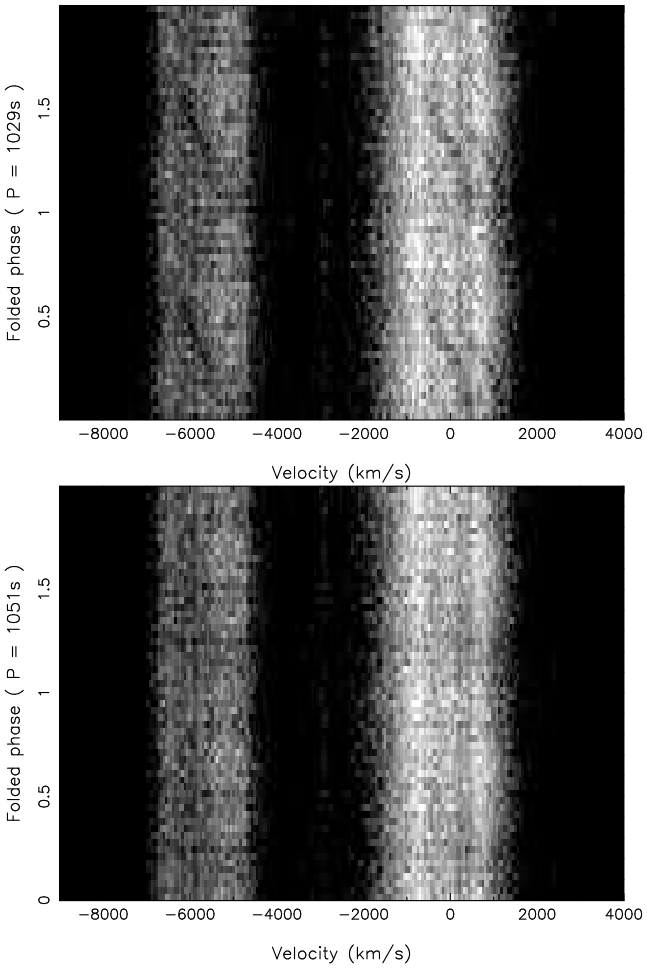

Figure 3. Trailed spectrogram of the He I 4387 and 4471 Å line profiles (absorption in white). **Top:** after folding on the candidate orbital period of 1028.73 s. **Bottom:** after folding on 1051.2 s. The gray scale is chosen in order to highlight the weak emission components in the core of the lines. A clear emission component is visible in both lines when the data are folded on 1029 s only, indicating that this is indeed the true orbital period of AM CVn.

(Fig. 2) reveals a clear peak around 3.5 cycles/hour, close to the expected orbital period of 17 minutes.

Because the accuracy of the candidate orbital periods as derived from the photometric studies of AM CVn exceeds the accuracy of our period determination using the EW lightcurve, we folded the data set on the two proposed orbital periods, 1028.73 s (Skillman et al., 1999) and 1051.2 s (Solheim et al., 1998). Both periods lie very close to the peak in our power spectrum.

An emission component is seen to be moving periodically through the line profiles when the spectra are folded on 1029 s, but not when they are folded on 1051 s (Figure 3). This S-wave is a characteristic signature in the line profiles of accreting binaries caused by the impact of the gas stream onto the accretion disc around the primary (e.g. Marsh, 1990; Spruit & Rutten, 1998; Marsh, 1999). The phase resolved spectroscopy thus provides a definite spectroscopic signature of the true orbital period of AM CVn, and firmly establishes its binary nature.

The S-wave is most clearly visible in the He I lines at

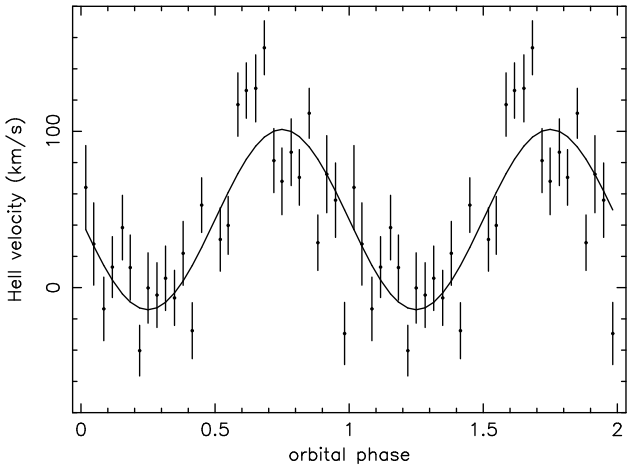

Figure 4. The radial velocities of the He II line, derived from a Gaussian fit as a function of orbital phase. A sinusoidal fit is used to establish the absolute orbital phases and derive an upper limit to the radial velocity of the primary.

4387 and 4471 Å, but can also be discerned in the line at 4143 Å. The He II lines at 4686 and 4199 Å, however, do not show any evidence for S-waves on the orbital period. The S-wave is strongest moving from redshift to blueshift, but only barely present when moving from blue to red. This reflects the fact that the hotspot is mainly visible when it is at the front of the system as observed from Earth. Note that when the spot comes to the front the velocity of the stream and of the disk at the impact point are directed away from the observer and thus redshifted.

3.2 Doppler tomography

As a next step we applied Doppler tomography in order to reveal the velocity structure in the lines as well as to establish the exact velocity of the S-wave. Doppler mapping (Marsh & Horne, 1988) uses the time dependent line profile shapes to reconstruct the distribution of line emission/absorption in the corotating frame of the binary. It is a widely applied tool in the study of the strong emission lines in CVs. It has revealed a variety of structures associated with the accretion disc around the primary in interacting binaries such as bright spots, spiral arms and magnetic streams (see for a review Marsh, 2001).

So far we have used an arbitrary zero point for our orbital phases since the absolute phase is not known from the photometry. In order to estimate the absolute orbital phase of the binary, where phase 0.0 is defined as superior conjunction of the primary star, we analysed the line profile behaviour when folded on the 1029 s orbital period. The line profiles are complex with a mix of absorption and emission components present at any given time. The He II 4686 Å line is an exception and consist of a single emission component superimposed on an absorption trough, and shows no evidence for an S-wave. We fitted the He II emission component with a simple Gaussian, in order to measure its radial velocity as a function of binary phase. The radial velocity of the He II line shows a systematic variation with an amplitude of 53 ± 6km s^{-1} when fitted with a simple sine-function (Fig. 4). If the emission is associated with the accretion flow around the primary, this gives us an indication of the motion of the primary white dwarf. Care must be taken since asymmetries in the distribution of the He II emission around the primary also introduces apparent radial velocity shifts. So rather than assuming that the derived velocity is indeed the projected velocity of the white dwarf (K_1), we merely use the relative phasing in order to construct a more reliable zero point for our phases. The derived velocity amplitude can be taken as an upper limit to the projected velocity of the white dwarf. Using the convention that orbital phase zero corresponds to superior conjunction of the primary, we then derive the following orbital ephemeris for AM CVn;

$$T_0(HJD) = 2450140.6135(2) + 0.011906623(3)E$$

with the formal uncertainty of the zero point indicated between brackets and the period taken from Skillman et al. (1999). In all plots, the orbital phases shown are the result of folding using the above ephemeris.

There are two methods of calculating Doppler tomograms from phase resolved spectroscopy. One is a straightforward back projection in conjunction with a Fourier filter (Horne, 1991), the other applies maximum entropy regularisation (Marsh & Horne, 1988). Our goal is to isolate the weak emission components in the cores of the He I absorption lines. To this end the filtered back projection method is preferred, since a maximum entropy reconstruction requires pure emission line profiles. Although more prone to reconstruction artifacts, the back-projection method can be applied to the complex line profiles of AM CVn without additional data processing. The results of back projecting the line profiles of the He I 4471 Å line are plotted in Fig. 5. Again we compare the back projection of the line profiles folded on the two periods; 1029 s and 1051 s. In the case of 1029 s, the S-wave maps into a prominent spot in the Doppler tomogram that is absent when folded on 1051 s. The location of the emission spot is where hotspot emission is expected, giving us confidence in the orbital ephemeris that is derived and our previous interpretation of the S-wave as due to the hotspot on the outer edge of the accretion disc.

3.3 The radial velocity of the mass donor

Apart from the hotspot itself, a weak ring of emission is visible in Fig. 5 from the rest of the accretion disc. At higher velocities this weak emission turns into absorption which produces the broad deep absorption wings in the lines. Having established the true orbital period of AM CVn, we can also constrain other system parameters using the position of the bright spot. The hotspot is the result of local heating and dissipation at the outer rim of the disc where the infalling gas stream impacts. In most cases, the emission has the velocity of the free falling stream (e.g. Marsh & Horne, 1990). However, in other cases the velocity of the hot spot gas appears to be a mix of the fall velocity as well as the local velocity flow in the disc at the impact point (Marsh, 1990). This unfortunately means that a straightforward fit to the position of the hotspot using single particle trajectories is unreliable. However, some interesting limits can still be obtained. First of all the velocity amplitude of the spot itself (403 ± 15 km s^{-1}) provides an upper limit to the possible projected velocity of the mass donor star (K_2), since the velocity of its centre of mass cannot be larger than that

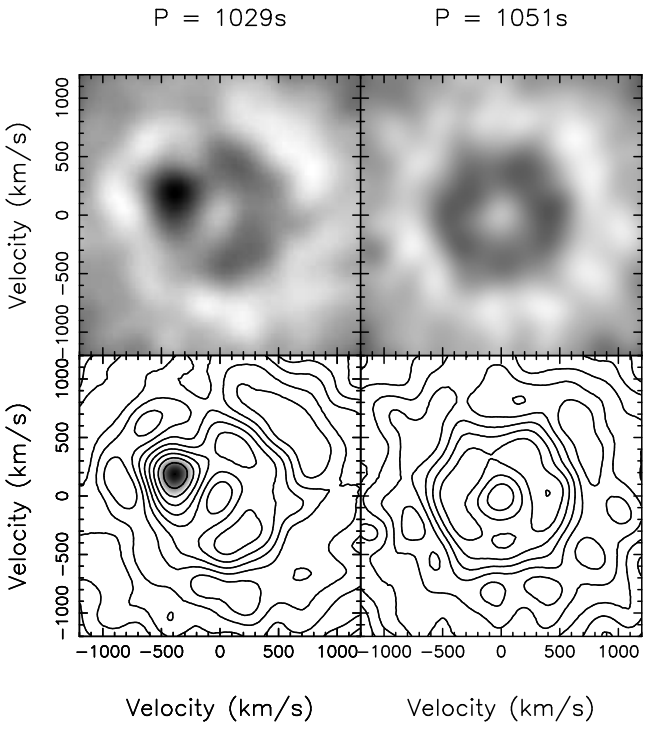

Figure 5. Filtered back-projection of the He I 4471 Å line profiles on the orbital period of 1029 s as well as the photometric period of 1051 s. The hotspot produces a prominent spot superposed on weak disc emission if folded on the correct period only. (Darker indicates more emission). The bottom two panels are the same images displayed as a contour plot. Any emission significantly brighter than the emission from the disc ring is overplotted as a gray scale, revealing the strong spot in the left tomogram.

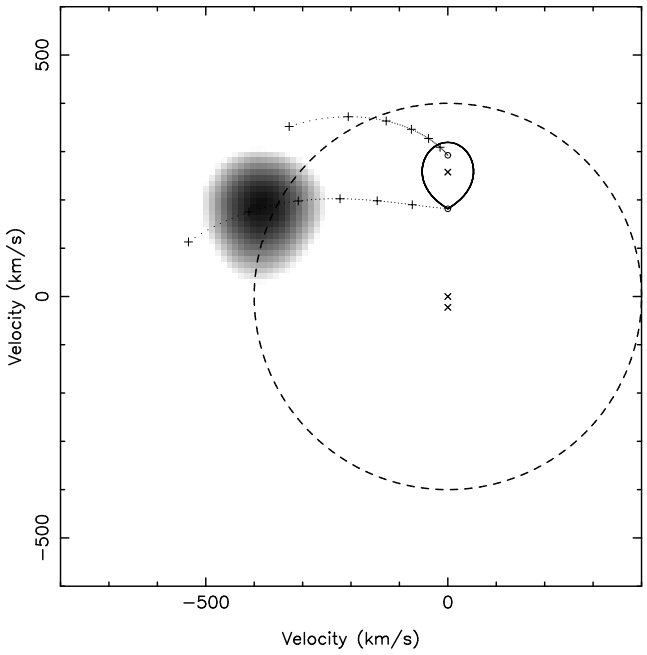

Figure 6. Ballistic trajectories that fit to the location of the hotspot. The observed position of the hotspot is plotted as a gray scale. Overplotted is the best fit ballistic stream trajectory, if the hotspot corresponds to pure free fall velocities. The corresponding velocities of the disc are indicated by the second trajectory above the ballistic one. The observed hotspot velocities need to lie in between these two trajectories for a given choice of K_2, leading to possible K_2 values between 210 and 265 km s^{-1}. The Roche lobed shape indicates the location of the mass donor star in the tomogram and the three crosses the centres of mass of the two components and the binary system.

of the hotspot itself. Very low values of K_2 also lead to gas stream trajectories that are incompatible with the data. For a given choice of K_1, K_2, we can calculate the trajectory of the gas stream as well as the velocity vector of the disc flow in order to isolate those parts in the tomogram where hot spot emission is possible. We shall see later that the mass ratio $q(= M_2/M_1)$ of AM CVn is most likely 0.087, which means that for a given choice of K_2, K_1 is derived from $K_1 = qK_2$.

If we assume that the hotspot velocities in AM CVn reflect the velocity of the ballistic gas stream, we can achieve a good fit to the observed tomogram using $K_2 = 260$ km s^{-1} and $K_1 = 23$ km s^{-1} (Fig. 6). If we relax our assumptions and only require that the observed velocities of the hotspot lie anywhere between the trajectory of the gas stream, and that of the disc, we can constrain K_2 to lie between 210 and 265 km s^{-1}. The assumed value of the mass ratio has only a small effect on the derived values for K_2.

The least constrained range for K_2 is obtained if we also consider the zero point of our orbital phases to be a free parameter. Then, in principle, K_2 can lie between 200 and 400 km s^{-1}. Note, however, that in order to fit the data with $K_2 > 280$ km s^{-1}, we need to apply an arbitrary phase shift in order for the stream to cross the hotspot, which also leads to an unrealistic impact radius that is very close to the white dwarf. We can thus firmly constrain the value of K_2 to lie between 210 and 280 km s^{-1}.

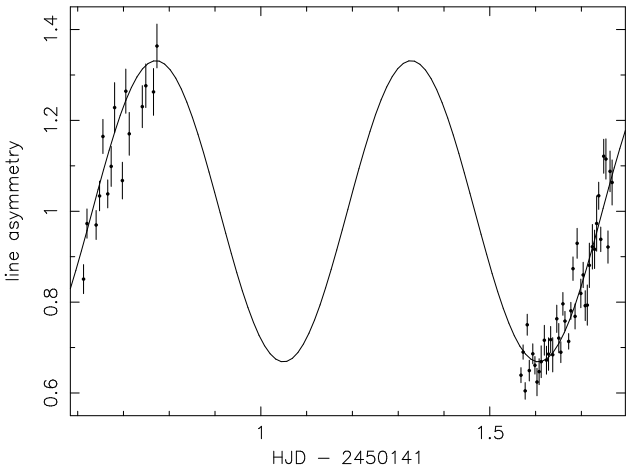

Figure 7. The change in relative absorption on the redshifted versus the blueshifted side across the 13.38 hour precession cycle. Plotted is the line asymmetry derived from a double Gaussian fit as a function of HJD. A least squares sinusoidal fit is overplotted.

3.4 Disc precession and superhumps

Patterson et al. (1993) have found a 13.38 hr period in the skewness of the He I absorption lines. From Fig. 1 we see indeed that the shape of the absorption lines changes during the 5 hrs of the total observation. This can be interpreted

as the varying double peaked absorption profiles of a precessing accretion disc (Patterson et al., 1993). We measured the skewness of the line profiles in our data by fitting multiple Gaussians to the absorption lines as follows. Since there is evidence for emission in the line cores, which modulates on the much shorter orbital period compared to the slow changes in the absorption lines on the precessing periods, the central emission was masked. Double Gaussians were fitted to the absorption components in order to measure the relative strength of the blue shifted absorption relative to the redshifted absorption. The spectra of both nights were grouped into bins of 10 consecutive spectra to improve signal to noise and the line asymmetry was measured accordingly. This double Gaussian method was found to be more reliable than calculating the formal skewness of the line as a whole since the emission components can be masked so as not to distort the measurements. Fig. 7 plots the derived line asymmetry together with a sinusoidal least squares fit. We do not cover the full precession cycle, so cannot improve on the precession period derived by Patterson et al. (13.38 hours) and fixed the period in the fit. The asymmetry is expressed as the ratio between the depths of both Gaussians. The relative contribution of the red versus blue shifted side of the disc thus changes with an amplitude of 33% across the precessing cycle. Adopting the very simple picture sketched in Patterson et al. (1993) using their ϕ_0 as phase, we coved phases 0.3 – 0.75 on the first night and phases 0.2 – 0.6 on the second night.

4 DISCUSSION

The fact that AM CVn behaves very similarly to the hydrogen rich superhump systems (Patterson et al., 1993) suggests that the superhump phenomena has the same origin (Warner, 1995). It could be explained by precession of an eccentric disk, which is caused by a tidal resonance between the disc and the companion which is found for mass transferring systems with a mass ratio smaller than 0.22 Whitehurst (1988) up to 0.33 (Murray, 2000). Simpson & Wood (1998) find a more complex behaviour of the disk, including disk shape changes and spiral shocks in the disk, but a similar 'precession' period. The numerical simulations of Hirose & Osaki (1990, 1993) show that there is a relation between the precession period, the orbital period and the mass ratio (Warner, 1995)

$$\frac{P_{\rm prec}}{P_{\rm orb}} = A\frac{1+q}{q} \qquad (1)$$

where $A \approx 3.73$ for systems with $q < 0.1$. Because of the tidal origin of the phenomenon there is no reason to expect a different relation for helium discs. Using 1028.73 s for the orbital period and 13.38 hr for the precession period, this relation gives a mass ratio for AM CVn of 0.087.

From the well known fact that for a Roche lobe filling star the period only depends on the mass and radius of the donor we can calculate the mass of the donor in AM CVn from the period and the mass – radius relation. From the two evolutionary scenarios that are proposed to lead to AM CVn stars, two mass – radius relations for the donor stars are found (Warner, 1995; Nelemans et al., 2001). From the mass ratio the companion mass is found. In Table 1 we give the two solutions for AM CVn using the mass – radius relation as given in Nelemans et al. (2001).

Table 1. System parameters for the two different mass radius relations: deg. for fully degenerate mass – radius relation for white dwarfs and semi for the semi-degenerate mass radius relation for the final products of helium CVs (from Tutukov & Fedorova, 1989, see Nelemans et al. 2001). The inclination is determined assuming $K_2 = 260$ km s^{-1}.

	M_2 ($M_\odot$)	M_1 ($M_\odot$)	K1/sin i (km s^{-1})	K2/sin i (km s^{-1})	i °
deg.	0.033	0.38	55.5	637.4	24.1
semi	0.114	1.31	83.7	961.8	15.7

From the system parameters we can calculate the radial velocities of the two components, which we can compare to the values of K_2 as derived from the Doppler tomograms. In Table 1 we give the expected values of the radial velocities ($K_{1,2}/\sin i$) and the resulting values for the inclination assuming $K_2 = 260$ km s^{-1}.

The derived inclinations are low, consistent with the fact that no eclipses are observed (which means $i < 78°$ for $q = 0.087$). The only clue to discern the two mass – radius relations (and thus the formation scenario) may be the fact that the hotspot is obscured when moving from blue to red, implying not too low inclination. This would slightly favour the fully degenerate mass radius relation. However the mass ratio derived from the superhump period is too uncertain to draw firm conclusions.

The value of K_1 derived from the mass ratio of 0.087 (23 km s^{-1}) seems incompatible with the interpretation of the radial velocity of the He II line as being caused by the motion of the primary. However it could be that the mass ratio determined from the superhump period is incorrect for AM CVn. For example for a mass ratio of 0.2, the value of K_1 would be 52 km s^{-1}. This also would bring the mass of the primary down, which rules out the fully degenerate mass – radius relation, but gives somewhat more realistic value for the primary mass in the case of the semi-degenerate mass – radius relation (see for more details Nelemans et al., 2001).

Evidence for time variability of the strength of the hot spot was found by folding both nights separately. Using the the first night only, no discernible S-wave could de identified. However, the second night alone, resulted in a clearly visible S-wave in several lines. Maybe the hot spot strength varies with the precession period, allthough the precession phase shift between the two nights is small. The poor quality of the data of the first night makes it for the moment impossible to draw conclusions. Better sampling of the precession period offers opportunities to study the strength and position of the hot spot as a function of the precession cycle, allowing a better determination of the hot spot position and thus the mass ratio provided adequate signal to noise can be obtained.

5 CONCLUSION

We found a clear S-wave in spectra of AM CVn when folded on a period of 1029 s, confirming the binary nature of AM

CVn beyond any possible remaining doubt and establishing 1028.73 s as the true orbital period.

The dominant photometrical period of 1051.2 s can be interpreted as the beat between the orbital period and the 13.38 hr period that has been found in the skewness of the absorption lines, making the system the helium equivalent of the permanent superhump systems. The 13.38 hr period then is interpreted as the precession period of the accretion disc. The shape of the absorption lines in our data set changes on the same period.

By applying Doppler tomography we were able to constrain the value of K_2 between 210 and 265 km s^{-1}, which given the formation channels implies a low inclination (between $\sim 15^\circ$ and $\sim 25^\circ$).

Our results open a new field of studying the details of these intriguing ultra-compact binaries by phase resolved spectroscopy and Doppler tomography.

ACKNOWLEDGMENTS

We thank Tom Marsh for motivating discussion and the use of the MOLLY data reduction package and the referee M. Wood for valuable comments. The William Herschel Telescope is operated on the island of La Palma by the Isaac Newton Group in the Spanish Observatorio del Roque de los Muchachos of the Instituto de Astrofisica de Canaria. This paper makes us of data obtained from the Isaac Newton Group Archive which is maintained as part of the Astronomical Data Centre at the Institute of Astronomy, Cambridge. GN is supported by NWO Spinoza grant 08-0 to E. P. J. van den Heuvel, DS is supported by a PPARC Fellowship and PJG is supported by a CfA fellowship.

REFERENCES

Faulkner J., Flannery B.P., Warner B., 1972, ApJ 175, L79
Greenstein J.L., Matthews M.S., 1957, ApJ 126, 14
Harvey D.A., Skillman D.R., Kemp J., et al., 1998, ApJ 493, L105
Hirose M., Osaki Y., 1990, PASJ 42, 135
Hirose M., Osaki Y., 1993, PASJ 45, 595
Horne K., 1991, in Shafter A.W., ed., Proc. 12. N. AM Worksh. on CVs & XRBs, p. 23
Humason M.L., Zwicky F., 1947, ApJ 105, 85
Marsh T.R., 1990, ApJ 357, 621
Marsh T.R., 1999, MNRAS 304, 443
Marsh T.R., 2001, in Boffin H., Steeghs D., Cuypers J., eds., Astro-tomography, Lecture Notes in Physics, Springer Verlag, in press, astr-ph/0011020
Marsh T.R., Horne K., 1988, MNRAS 235, 269
Marsh T.R., Horne K., 1990, ApJ 349, 593
Murray J.R., 2000, MNRAS 314, L1
Nelemans G., Portegies Zwart S.F., Verbunt F., Yungelson L.R., 2001, A&A 368, 939
Paczyński B., 1967, Acta Astron. 17, 287
Patterson J., Halpern J., Shambrook A., 1993, ApJ 419, 803
Simpson J.C., Wood M.A., 1998, ApJ 506, 360
Skillman D.R., Patterson J., Kemp J., et al., 1999, PASP 111, 1281
Smak J., 1967, Acta Astron. 17, 255
Solheim J.E., Provencal J.L., Bradly P.A., et al., 1998, A&A 332, 939
Solheim J.E., et al., 1991, in Vauclair G., Sion E.M., eds., White Dwarfs, p. 431, Kluwer, Dordrecht
Spruit H.C., Rutten R.G.M., 1998, MNRAS 299, 768
Tutukov A.V., Fedorova A.V., 1989, SvA 33, 606
Warner B., 1995, Ap&SS 225, 249
Warner B., Robinson E.L., 1972, MNRAS 159, 101
Whitehurst R., 1988, MNRAS 232, 35